Atomic photoionization and dynamical stabilization with subrelativistically intense high-frequency light: Magnetic-field effects revisited

M. Yu. Emelin[1,2,*] and M. Yu. Ryabikin[1,2]

[1]*Institute of Applied Physics, Russian Academy of Sciences, Nizhny Novgorod 603950, Russia*

[2]*Lobachevsky State University of Nizhny Novgorod, Nizhny Novgorod 603950, Russia*

(Received 9 October 2013; published 21 January 2014)

The results of three-dimensional numerical simulations of strong-field atomic stabilization with arbitrarily polarized light beyond the electric dipole approximation are presented. The study of the long-term evolution of the ground-state hydrogen atom exposed to an intense high-frequency laser field reveals the persistence of the metastable bound states up to relativistic intensities. The population of these states in a pulsed field is examined as a function of the pulse peak intensity. These calculations resolve recent contradictions in the literature related to the role of magnetic field in the high-frequency stabilization phenomenon.

DOI: 10.1103/PhysRevA.89.013418 PACS number(s): 32.80.Fb, 42.50.Hz

I. INTRODUCTION

The theory of atomic photoionization in an intense high-frequency laser field is known to predict the counterintuitive phenomenon of stabilization, i.e., the saturation or even the decrease of ionization probability with increasing laser intensity [1,2]. So far, laser sources permitting the observation of atomic stabilization in ground-state tightly bound atomic systems were not available. Thanks to recent advances in free-electron laser technology, the short-pulse coherent light sources producing VUV and soft-x-ray pulses with peak intensity higher than 10^{17} W/cm^2 become available, which are expected to allow experimental observation of the atomic high-frequency stabilization. This to a large extent determines the recently renewed interest in this unusual phenomenon [3–7].

Although the basic mechanisms and many aspects of atomic stabilization have been well studied theoretically, some important issues remain unresolved. Of fundamental significance are those related to the role of the magnetic field of the laser pulse for intensities reaching weakly relativistic regime. On the one hand, both the classical Monte Carlo simulations [8] and quantum-mechanical numerical experiments [9,10] have indicated that the magnetic field pushing the electron away from the nucleus in the laser pulse propagation direction hampers stabilization, thereby reducing to a rather narrow window the intensity range in which the atom is relatively stable against ionization. On the other hand, using the relativistic strong-field approximation (RSFA) [11] to study analytically the stabilization of the hydrogen atom in a very intense linearly [12] and circularly [13] polarized field, Reiss showed that (i) the H atom is increasingly stable against ionization as the laser intensity increases and (ii) the relativistic effects enhance stabilization. As stated in [13], this contrast poses an interesting contradiction that needs to be resolved. In this article, we present the results of quantum-mechanical numerical simulations, which are to address thoroughly these issues and shed light on the above-mentioned contradiction.

Most previous numerical studies of atomic stabilization have been carried out within the context of reduced-dimensionality models, which allow one to dramatically reduce the computational efforts [9,10,14–16]. In particular, the two-dimensional (2D) models, which contained the essential physics of their full-dimensionality counterparts, allowed the numerical studies of atomic stabilization in arbitrarily polarized laser fields employing the electric dipole approximation [10,15,16], as well as the nondipole simulations for the case of linearly polarized field [9,10] to be carried out. The latter approach, however, was one of the subjects of criticism in [13] where the validity of the 2D theory to describe the intrinsically three-dimensional (3D) phenomena, such as those originating from the coupled electric and magnetic fields, has been put into question.

Three-dimensional numerical studies of ionization processes in the high-intensity laser field are, in general, computationally demanding. The exception is the case of a linearly polarized field, for which the cylyndrical symmetry of the problem can be exploited to reduce the computational efforts when the electric dipole approximation is assumed; the corresponding numerical 3D studies of atomic stabilization for ground-state hydrogen can be found, e.g., in [17,18]. For the more demanding case of circular polarization, several 3D numerical studies of stabilization, both within [19–21] and beyond [22,23] the dipole approximation have been reported to date; however, these studies were generally restricted to very short pulses (typically no longer than 10 cycles). Furthermore, in the nondipole case the 3D studies are scarce: For both linear and circular polarizations, only very few specific values of the laser parameters have been addressed.

In this paper, we present the results of numerical simulations for the dynamic stabilization of ground-state hydrogen in the arbitrarily polarized pulsed laser field, including the magnetic-field effects, in full (3D) dimensionality. The long-term evolution of the electron wave function for a wide range of laser intensities is addressed.

The paper is organized as follows. In Sec. II we briefly describe the details of our numerical calculations in the dipole and nonrelativistic nondipole approximations. The numerical results are presented in Sec. III. In Sec. IIIA the results of 3D calculations of the H atom survival probability in a short laser pulse are presented and compared with those obtained earlier within the reduced-dimensionality models; the results for different laser polarizations are also discussed. In Sec. IIIB the evolution of the H atom exposed to a very long circularly

*emelin@ufp.appl.sci-nnov.ru

polarized laser pulse is studied numerically and discussed in terms of the field-dressed states and transitions between them. The detailed study of the long-term evolution of the part of the electron wave packet, which remained localized after the field switching-on, is presented. The comparison between the dipole and nondipole results for the ionization rate in the asymptotic regime is presented in Sec. IIIC for both linear and circular polarizations of the field. An interpretation of the nonrelativistic nondipole results in terms of the laser-dressed Coulomb potential and their relations with other existing theories are discussed in Sec. IV. Section V contains concluding remarks.

II. NUMERICAL METHOD

For the sake of comparison, the calculations were performed both within the electric dipole approximation and beyond it. In the first case, we solved the time-dependent Schrödinger equation (TDSE), in which the vector potential $\boldsymbol{A}$ of the electromagnetic field is assumed to be only time dependent. In the second case, the laser field was described by the spatially dependent vector potential $\boldsymbol{A}(t - z/c)$, which corresponds to the laser pulse traveling in the positive z direction. Taking into account the smallness of the localization scale of the electron wave packet in comparison with the laser wavelength, we used an approximate form for $\boldsymbol{A}(t - z/c)$ retaining only the first-order retardation correction beyond the dipole approximation $\boldsymbol{A}(t)$ [10,24]. In this case, through a unitary transformation, the initial equation can be reduced to the form (hereinafter, we use atomic units),

$$i\frac{\partial\Psi}{\partial t} = -\frac{1}{2}\left(\frac{\partial^2}{\partial x^2}+\frac{\partial^2}{\partial y^2}+\frac{\partial^2}{\partial z^2}\right)\Psi - i\left(v_x\frac{\partial}{\partial x}+v_y\frac{\partial}{\partial y}+v_z\frac{\partial}{\partial z}\right)\Psi - \frac{1}{r}\Psi, \quad (1)$$

with $v_{x,y} = A_{x,y}(t)/c$ and $v_z = (v_x^2 + v_y^2)/(2c)$, where v_z is the z component of the classical electron velocity calculated in the lowest order in $1/c$. This equation differs from its dipole-approximation counterpart by an additional term $-iv_z(\partial\Psi/\partial z)$ describing the motion of an electron along the z axis due to the coupled electric and magnetic fields. We neglect the spin of the electron, since for the laser parameters of interest here the coupling of the magnetic laser field to the spin leads only to small-amplitude spin oscillations, which do not affect ionization significantly, as shown in calculations carried out to first order in $1/c$ via the Pauli equation [25,26].

In both cases, the TDSE was integrated numerically using the fast Fourier transform-based split-operator technique [27]. The calculations were performed using a multithreaded numerical code we have created on the basis of libraries implementing the POSIX Threads standard.

The calculations were made for the laser field $\boldsymbol{E}(t) = -(1/c)\partial\boldsymbol{A}(t)/\partial t = \boldsymbol{e}_x E_x(t) + \boldsymbol{e}_y E_y(t)$ with $E_x(t) = Ef(t)\sin\omega t$, $E_y(t) = \varepsilon E_x(t - T/4)$, where E, ω, $T = 2\pi/\omega$ and ε are the electric field amplitude, angular frequency, period, and ellipticity, respectively; the field envelope is trapezoidal with n_r-cycle linear ramps and n_c-cycle interval of constant amplitude [(n_r-n_c-n_r) pulse]:

$$f(t) = \begin{cases} t/(n_rT), & 0 < t/T \leqslant n_r \\ 1, & n_r < t/T \leqslant n_r + n_c \\ (2n_r + n_c - t/T)/n_r, & n_r + n_c < t/T \leqslant 2n_r + n_c \\ 0, & t/T \notin [0, 2n_r + n_c]. \end{cases} \quad (2)$$

The calculations were performed on a grid centered at the nucleus, with absorbing boundaries used to avoid wave-function reflections from the edges. The probability for the electron to remain localized around the nucleus was calculated as the norm of the wave function over the cube with an edge length exceeding $4\alpha_0$ (we will call it the "inner region"), where $\alpha_0 = E/\omega^2$ is the maximum classical displacement of an electron.

III. NUMERICAL RESULTS

A. Atom survival probability in short laser pulse with arbitrary polarization

Figure 1 shows the results of 3D simulations for the ground-state H atom exposed to the circularly [Fig. 1(a)] and linearly [Fig. 1(b)] polarized field with the same time profile as in the 2D numerical study [10] of atomic stabilization in a linearly polarized field. The laser pulse is trapezoidal (2-10-2) pulse; the angular frequency is $\omega = 1$ a.u. The atom survival probability shown in Fig. 1 is the norm of the time-dependent wave function calculated 14 cycles past the end of the pulse, when the changes in this norm become negligible. This probability is plotted as a function of the laser peak intensity

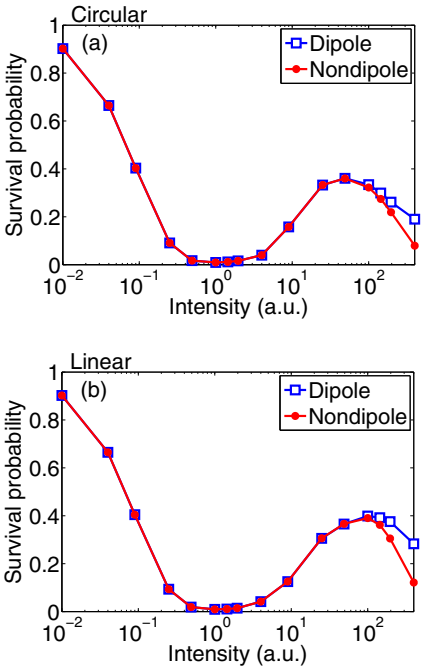

FIG. 1. (Color online) Atom survival probability for a 14-cycle pulse with $\omega = 1$ a.u. vs laser peak intensity $I = E^2(1 + \varepsilon^2)$. Dipole (blue open squares) and nondipole (red circles) results are shown for (a) circular and (b) linear polarization.

$I = E^2(1+\varepsilon^2)$; dipole and nondipole results are shown for both polarizations.

Comparison of the 3D results in Fig. 1(b) with those obtained within the reduced-dimensionality hydrogenlike models for the same laser pulse parameters [10,28] shows that the dimensionality has no decisive influence on the very existence of the atomic stabilization effect as well as on the extension of the stabilization window (the stabilization effect is manifested in Fig. 1 as an increase in the atom survival probability for the laser intensities between approximately 1 and 50–100 a.u.; this intensity range is called the "stabilization window"). Although the width and depth of the "death valley" (the region around the minimum of the atom survival probability) increase with the dimensionality of the model, the position of the minimum of the atomic survival probability is about the same for one-dimensional (1D), 2D, and 3D cases; also the same for 2D and 3D cases is the value of the intensity, starting from which the effect of the magnetic field leads to a reduced survival probability as compared to what would be expected from a dipole-approximation consideration. Moreover, for both dipole and nondipole cases, the results for different laser polarizations are also close to each other [cf. Figs. 1(a) and 1(b)].

To discuss further the issues raised in [13], we will consider in detail the case of a circularly polarized laser pulse. This analysis will be based on a series of 3D simulations of the long-term evolution of the ground-state H atom exposed to a very long trapezoidal laser pulse [(2-200-2) pulse] with carrier frequency $\omega = 4$ a.u.

B. Long-term evolution of the H atom

Figure 2 shows, for different peak intensities of the circularly polarized laser field, the time evolution of the probability to find an electron localized in the inner region; in all cases shown are the results obtained both in the dipole approximation and beyond it. The case shown in Fig. 2(a) corresponds to a laser intensity lying within the H atom stabilization window for $\omega = 4$ a.u. The difference between the dipole and nondipole calculations in this case is small and the behavior of the atomic electron is very close to that familiar from the dipole approximation, in which it is known to be conveniently described in terms of the Kramers-Henneberger (KH) states [1,29]. KH states arise in the theory of atomic stabilization as a result of the application of the high-frequency Floquet theory (HFFT) to the TDSE transformed to the KH frame, which is the rest frame of the classical electron in the ac electric field $E(t)$. In lowest order in ω^{-1}, HFFT describes atomic states in an intense high-frequency field as the stationary dressed states (KH states) in the effective static potential $V_0(\boldsymbol{\alpha}_0, \boldsymbol{r}) = (1/T)\int_0^T V(\boldsymbol{r}+\boldsymbol{\alpha}(t))dt$, which is the cycle-averaged oscillating Coulomb potential $V(\boldsymbol{r}+\boldsymbol{\alpha}(t)), \boldsymbol{\alpha}(t) = (1/c)\int_{-\infty}^{t} \boldsymbol{A}(t')dt'$. The harmonics of the potential $V(\boldsymbol{r}+\boldsymbol{\alpha}(t))$ are, in the KH picture, responsible for ionization.

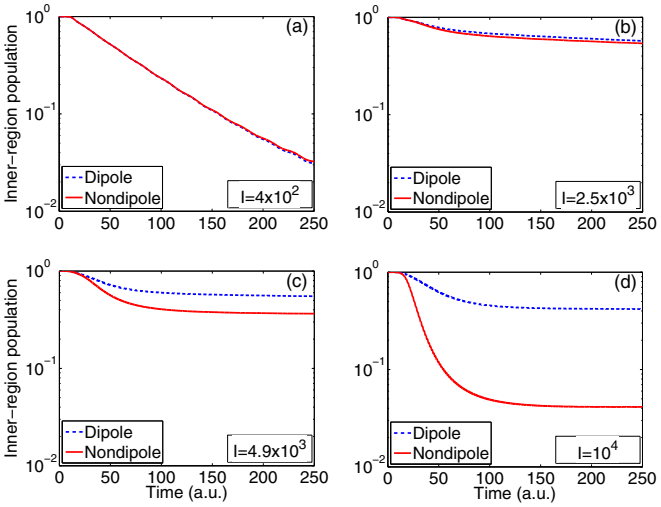

FIG. 2. (Color online) Long-term behavior of the inner-region population for a 204-cycle (≈320 a.u.) circularly polarized laser pulse with $\omega = 4$ a.u. and different peak intensities (see legends). Dipole (blue dotted curve) and nondipole (red solid curve) results are shown.

For a circularly polarized field, the effective potential is a circular trough of radius α_0; the probability distribution in the ground KH state then has a toroidal shape [15,30]. In the laboratory frame, this torus rotates around the Coulomb center like a hoop twirling around the dancer's waist [19]. For a quickly ramped laser pulse considered here, the dynamics of an electron is more complicated because of "shake-up" processes described within the HFFT as the nonadiabatic transitions to excited Floquet eigenstates. Since the system is shaken up into a superposition of discrete Floquet states with different azimuthal quantum numbers and quasienergies, the probability density is nonuniformly distributed in a time-dependent manner along the ring [20].

Figures 2(b)–2(d) show how the behavior of the inner-region population changes as the laser intensity goes beyond the above-mentioned regime. Both dipole and nonrelativistic nondipole simulations (note that the maximum classical electron velocity for the calculations shown in Fig. 2 does not exceed 0.13 c, which justifies the use of a nonrelativistic approach) show that the dynamics of the system now follows a generic scenario that includes two successive stages: (i) rapid loss of a bound-state population due to the "shake-off" into the continuum during the turn-on of the field and (ii) smooth decay because of the steady transfer of population to the continuum due to ionization from the superposition of populated bound states.

At high laser intensities, the inner-region depopulation at the stage (i) is enhanced dramatically in the nondipole case compared with the dipole calculations. This is the consequence of the photon momentum transfer taken into account in the calculations beyond the dipole approximation [31]. As the laser intensity increases, more photons can be involved in the Raman transitions giving rise to the "shake-up" and "shake-off" processes. The resulting larger net momentum transfer leaves the electron less chance to remain bound to the Coulomb center. As a result, a significant part of the electron wave packet is pushed away from the nucleus; see Fig. 3(a) (the snapshot taken at stage (i) captures a particlelike electron subpacket escaping along a helical path from the core to the upper border of the box displayed in the figure). The rest of the population after the field turn-on remains localized

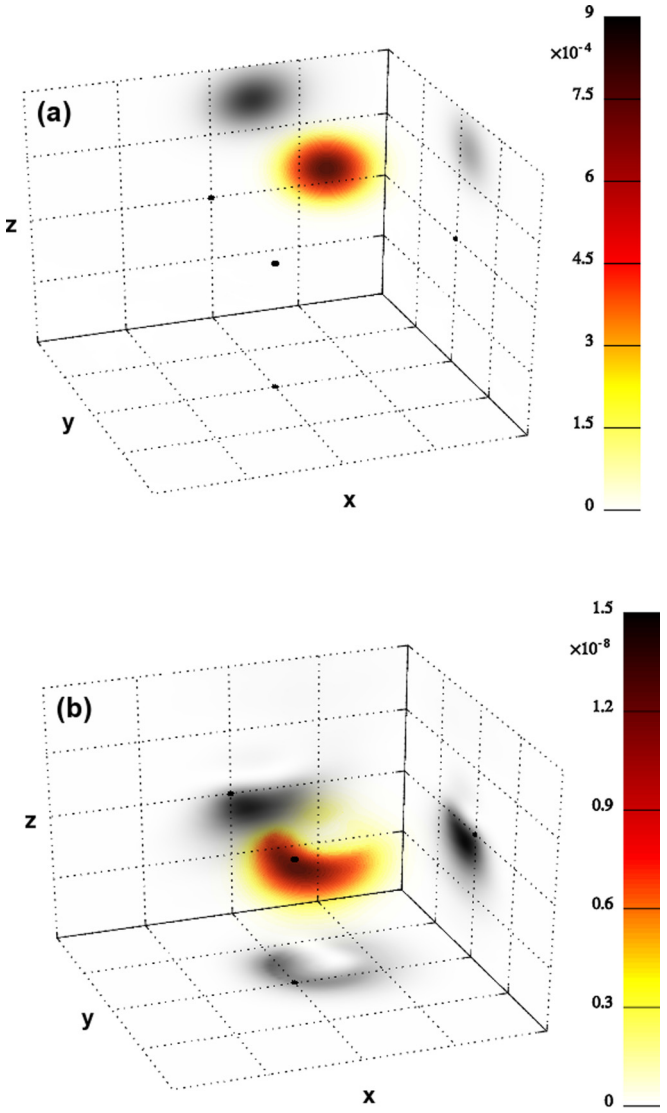

FIG. 3. (Color online) (a) Delocalized and (b) localized parts of the electron wave packet for the H atom driven by a circularly polarized laser pulse with $\omega = 4$ a.u. and $I = 2.25\times10^4$ a.u. (nondipole results). The snapshots in (a) and (b) are taken at $t \approx 10$ a.u. and $t \approx 250$ a.u., respectively. The color scale for the probability density differs between (a) and (b) by a factor of 6×10^4. Shown on the coordinate planes are the contour plots of the probability density in the mutually orthogonal planes passing through the nucleus. The grid line spacing is 12.8 a.u.; a proton is at the origin.

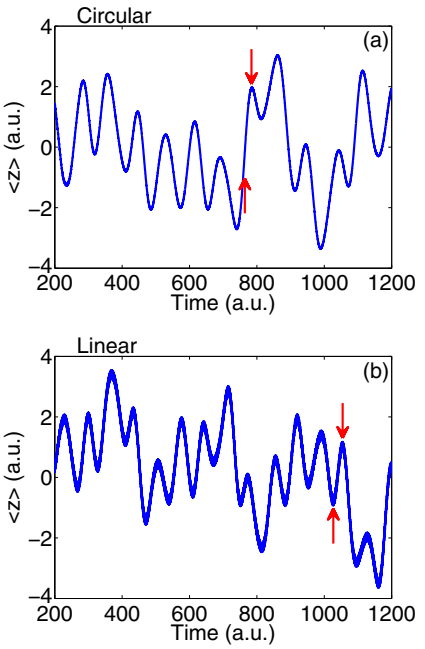

FIG. 4. (Color online) Long-term behavior of the expectation value of the electron's coordinate along the laser pulse propagation direction for the localized part of electron wave packet. Nondipole results are shown for (a) circularly and (b) linearly polarized laser pulse with $\omega = 4$ a.u. and $I = 10^4$ a.u.

near the nucleus; see Fig. 3(b) [the snapshot is taken long after the delocalized part of the electron wave packet has drifted beyond the box, stage (ii). Note the large difference in color scales between Figs. 3(a) and 3(b)]. The probability for the atomic bound electron to remain localized after the field switching-on depends strongly on the shape of the rising edge of the pulse [32]. For example, for $I = 4.9\times10^3$ a.u. the inner-region population at the time instant $t = 100$ a.u. is 0.406 for our trapezoidal pulse [see Fig. 2(c)], whereas for the flat-top pulse with Gaussian-shaped edges, this value is 0.205, 0.438, and 0.535 for the turn-on width at half maximum of intensity equal to 1, 2, and 4 cycles, respectively.

The localized population demonstrates slow decay approaching asymptotically an exponential law as time goes to infinity. In this limit, the slow shaken-off electrons no longer contribute to the inner-region population, so the temporal evolution of the depopulation of this region in the asymptotic regime provides a highly accurate value of the rate of ionization from the bound states.

The behavior of the localized part of the electron wave packet is now not the same as in the dipole approximation but rather resembles the motion of the hoop as the dancer performs the "corkscrew" trick: The electron now not only rotates around the nucleus but also takes an excursion back and forth along the z axis [see Figs. 4(a) and 5(a) showing, respectively, the time dependence of the z coordinate of the electron wave-packet center of mass and the fragment of the 3D trajectory for this case].

C. Ionization rate in the asymptotic regime

An inspection of the inner-region population decay at the stage (ii) reveals, opposed to the stage (i), no visible difference between the dipole and nondipole results [cf. blue dotted and red solid curves in Figs. 2(b)–2(d)]. This is shown more explicitly in Fig. 6(a) that plots the ionization rates in the asymptotic regime vs the intensity of a circularly polarized laser field. The ionization rates were calculated by fitting the exponential function to the numerical data for inner-region population at large t. The calculations have been done up to the intensities beyond which the higher-order corrections in $1/c$ should be taken into account.

A similar analysis was also done for other laser polarizations. The results turn out to be, in general, very similar to those

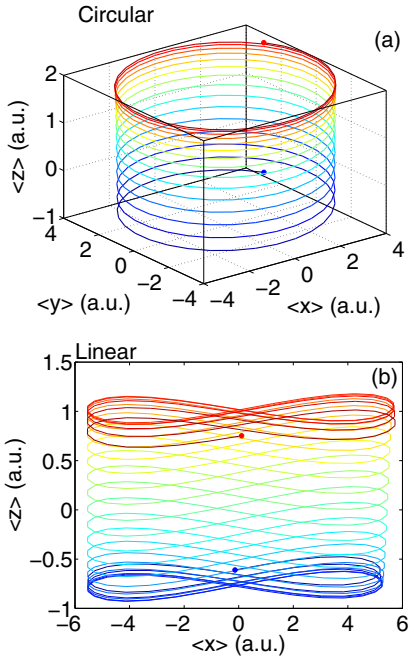

FIG. 5. (Color online) Center-of-mass trajectory for the localized part of the electron wave packet in the (a) circularly and (b) linearly polarized laser pulse with $\omega = 4$ a.u. and $I = 10^4$ a.u. The relevant time intervals are depicted by arrows in Fig. 4.

for a circular polarization. This is in spite of the fact that the structures of the stabilized states in the linear and circular cases are quite different and the nondipole center-of-mass trajectory of the localized electron wave packet in the linear case is essentially 2D instead of 3D. This is the drifting "eight-figure" motion [see Fig. 5(b)]. The spatial extent in x of the trajectory shown in Fig. 5(b) is 11.4 a.u., which agrees satisfactorily with the KH picture (the deviation from $2\alpha_0 = 12.5$ a.u. can be explained by the contributions of excited dressed states), whereas the width of the "figure eight" is 0.285 a.u., which agrees perfectly with the exact solution [33] of the relativistic equation of motion for the classical electron in the plane-wave field. This trajectory in the linear case exhibits the same slow oscillations along the z axis as in the circular case [cf. Figs. 4(a) and 4(b)]. Note also that the curve in Fig. 4(b) looks thicker; this is because the movement along the z coordinate in this case also includes small-scale oscillations at a frequency 2ω; see Fig. 5(b). Moreover, the ionization rate in the asymptotic regime behaves with increasing laser intensity in the same way for any laser polarization. In particular, the slope of the straight lines in Figs. 6(a) and 6(b) is the same, whereas the value of the ionization rate for the linear case is on average only about 1.3 times larger than in the circular case. Most importantly, in all cases the ionization rate in the asymptotic regime shows no influence of the magnetic field.

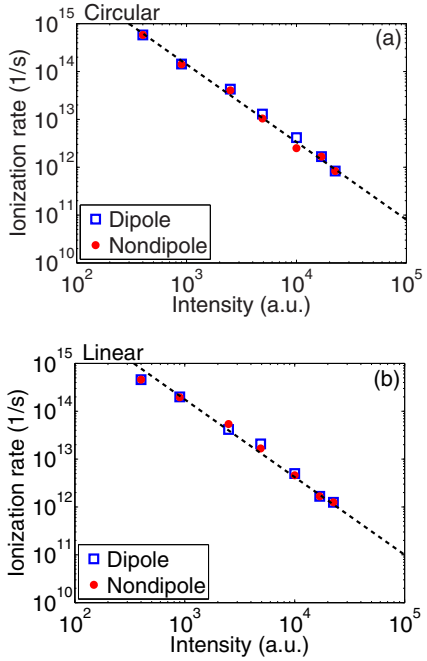

FIG. 6. (Color online) Ionization rate vs laser peak intensity for H atom at $\omega = 4$ a.u. in the asymptotic regime. Dipole (blue open squares) and nondipole (red circles) results are shown for (a) circular and (b) linear polarization.

IV. DISCUSSION

The results in Figs. 3–6 can be interpreted in terms of the laser-dressed Coulomb potential, which is the generalization of the KH potential taking into account the relativistic and higher multipole effects. For linear polarization, this generalization was proposed in Ref. [34]. In this case, the laser-dressed Coulomb potential is singular along a figure eight rather than a straight line. Our study shows that the nonadiabatic switching of the laser field creates the superposition of bound states in this eight-shaped potential, thereby giving rise to the electron wave-packet center-of-mass motion shown in Figs. 4(b) and 5(b). Note, however, that the scale in Fig. 5(b) differs between the x and z axes by a factor of four, so even for intensity as high as $I = 10^4$ a.u., the eight figure is very much flattened. This is the manifestation of the fact that for the intensity range explored above, the nondipole corrections to the KH potential are still very small. This conclusion agrees with the estimation [34] that for $\alpha_0 < 147(2\omega)^{-3/4}$ (in atomic units) the nonrelativistic dipole treatments by Gavrila and coworkers for the metastable bound states (see [1] and references therein) are valid; for the case of $\omega = 4$ a.u., the above-mentioned condition is fulfilled for $I < 2.4 \times 10^5$ a.u.

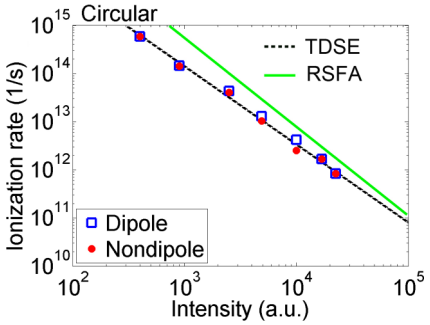

FIG. 7. (Color online) Same as in Fig. 6(a) plotted against the RSFA relativistic calculations from [13].

One can expect that in this intensity range not only the cycle-averaged potential but also the harmonics of the oscillating Coulomb potential are not yet distorted too strongly to lead to visible difference between the dipole and nondipole results for the ionization rate [32], which is indeed the case; see Fig. 6(b).

Although the calculations in [34] were limited to the case of linear polarization, this treatment may be likely generalized to an arbitrary polarization. Our study has revealed that, for a wide range of intensities beyond the nonrelativistic dipole regime, the metastable bound states persist for any polarization with the lifetimes comparable to those for the linear polarization. Whereas the nondipole corrections lead to the above-mentioned qualitative changes of the bound-electron wave-packet evolution, they, just like for the linear polarization case, do not result in significant changes of the ionization rate.

Now it is interesting to compare the bound-state population decay rates shown in Fig. 6 with the ionization rates calculated using the RSFA [13]. In the latter approximation, by the way, the ionization rates for both nonrelativistic and relativistic cases turn out to agree perfectly with the results of the nonrelativistic HFFT theory [35] in a wide range of laser intensities. For comparison, the results of our TDSE numerical simulations for $\omega = 4$ a.u. are plotted in Fig. 7 against the RSFA calculations. Good qualitative agreement between these calculations is seen. The quantitative differences in the ionization rates can be explained by the slower ionization of the excited Floquet states [36] contributing in our case compared to the ground state addressed in [13,35].

V. CONCLUSION

In conclusion, in this work the extensive full-dimensionality nondipole numerical simulations of high-frequency stabilization of the hydrogen atom with an arbitrarily polarized pulsed laser field have been performed. Our study provides direct evidence that a set of metastable bound states of the system persists up to relativistic intensities, whose lifetimes increase with the intensity and do not depend significantly on the laser polarization and the magnetic field of the pulse. For intensities exceeding the critical level determined by the net momentum transfer from the incoming photons to the electron, the population of the metastable states decreases quickly with the intensity. It's worth noting, however, that the latter effect depends strongly on the shape of the rising edge of the laser pulse. Future technologies of the soft-x-ray pulse shaping can be therefore expected to facilitate experimental observation of the atomic high-frequency stabilization in a relativistically strong laser field. We believe our study is helpful for understanding the dynamics of an atom in intense high-frequency pulsed laser fields and bridging the gap between the existing theories and *ab initio* numerical simulations.

ACKNOWLEDGMENTS

We acknowledge financial support from the RFBR (Grants No. 12-02-31325 and No. 12-01-31270), Ministry of Education and Science of RF (Contract No. 11.G34.31.0011), and Presidential Council on Grants of RF (Grant No. 2001.2014.2).

[1] M. Gavrila, J. Phys. B **35**, R147 (2002).
[2] A. M. Popov, O. V. Tikhonova, and E. A. Volkova, J. Phys. B **36**, R125 (2003).
[3] K. Toyota, O. I. Tolstikhin, T. Morishita, and S. Watanabe, Phys. Rev. Lett. **103**, 153003 (2009).
[4] T. Birkeland, R. Nepstad, and M. Førre, Phys. Rev. Lett. **104**, 163002 (2010).
[5] S. A. Sørngård, S. Askeland, R. Nepstad, and M. Førre, Phys. Rev. A **83**, 033414 (2011).
[6] H. Ebadi, C. H. Keitel, and K. Z. Hatsagortsyan, Phys. Rev. A **83**, 063418 (2011).
[7] S.-S. Wei, S.-Y. Li, F.-M. Guo, Y.-J. Yang, and B. Wang, Phys. Rev. A **87**, 063418 (2013).
[8] C. H. Keitel and P. L. Knight, Phys. Rev. A **51**, 1420 (1995).
[9] N. J. Kylstra, R. A. Worthington, A. Patel, P. L. Knight, J. R. Vázquez de Aldana, and L. Roso, Phys. Rev. Lett. **85**, 1835 (2000).
[10] M. Y. Ryabikin and A. M. Sergeev, Opt. Express **7**, 417 (2000).
[11] H. R. Reiss, J. Opt. Soc. Am. B **7**, 574 (1990).
[12] D. P. Crawford and H. R. Reiss, Opt. Express **2**, 289 (1998).
[13] H. R. Reiss, Opt. Express **8**, 99 (2001).
[14] Q. Su, J. H. Eberly, and J. Javanainen, Phys. Rev. Lett. **64**, 862 (1990).
[15] A. Patel, M. Protopapas, D. G. Lappas, and P. L. Knight, Phys. Rev. A **58**, R2652 (1998).
[16] A. Patel, N. Kylstra, and P. L. Knight, Opt. Express **4**, 496 (1999).
[17] K. C. Kulander, K. J. Schafer, and J. L. Krause, Phys. Rev. Lett. **66**, 2601 (1991).
[18] M. Dondera, H. G. Muller, and M. Gavrila, Phys. Rev. A **65**, 031405 (2002).
[19] D.-I. Choi and W. Chism, Phys. Rev. A **66**, 025401 (2002).
[20] D. Bauer and F. Ceccherini, Phys. Rev. A **66**, 053411 (2002).
[21] M. Boca, H. G. Muller, and M. Gavrila, J. Phys. B **37**, 147 (2004).
[22] J. R. Vázquez de Aldana and L. Roso, Laser and Part. Beams **20**, 185 (2002).
[23] M. Førre, S. Selstø, J. P. Hansen, T. K. Kjeldsen, and L. B. Madsen, Phys. Rev. A **76**, 033415 (2007).
[24] A. V. Kim, M. Y. Ryabikin, and A. M. Sergeev, Phys. Usp. **42**, 54 (1999).
[25] O. Latinne, C. J. Joachain, and M. Dörr, Europhys. Lett. **26**, 333 (1994).
[26] J. R. Vázquez de Aldana and L. Roso, J. Phys. B **33**, 3701 (2000).
[27] J. A. Fleck, J. R. Morris, and M. D. Feit, Appl. Phys. **10**, 129 (1976).
[28] M. Y. Ryabikin and A. M. Sergeev, Laser Phys. **11**, 244 (2001).
[29] W. C. Henneberger, Phys. Rev. Lett. **21**, 838 (1968).
[30] M. Pont, Phys. Rev. A **40**, 5659 (1989).

[31] A. Bugacov, M. Pont, and R. Shakeshaft, Phys. Rev. A **48**, R4027 (1993).

[32] J. R. Vázquez de Aldana, N. J. Kylstra, L. Roso, P. L. Knight, A. Patel, and R. A. Worthington, Phys. Rev. A **64**, 013411 (2001).

[33] L. D. Landau and E. M. Lifshitz, *The Classical Theory of Fields*, 3rd ed. (Pergamon Press, Oxford, New York, 1971).

[34] P. S. Krstic and M. H. Mittleman, Phys. Rev. A **42**, 4037 (1990).

[35] M. Pont and M. Gavrila, Phys. Rev. Lett. **65**, 2362 (1990).

[36] M. Dörr, R. M. Potvliege, D. Proulx, and R. Shakeshaft, Phys. Rev. A **43**, 3729 (1991).